Lattice Lorentz gas: kinetic theory

1990 J. Phys. A: Math. Gen. 23 4953

(http://iopscience.iop.org/0305-4470/23/21/032)

J. Phys. A: Math. Gen. **23** (1990) 4953-4976. Printed in the UK

Lattice Lorentz gas: kinetic theory

G A van Velzen

Institute for Theoretical Physics, Princetonplein 5, PO Box 80006, 3508 TA Utrecht, The Netherlands

Received 22 March 1990

Abstract. Standard approximation schemes in kinetic theory are compared with the effective medium approximation (EMA), that was developed earlier for the stochastic Lorentz gas on cubic lattices. In models with reflecting collisions the low-density results are in strong disagreement with molecular chaos and in excellent agreement with the simulation data. The present analysis identifies the diagrams that are taken into account in the different approximations. The EMA accounts in a self-consistent way for *all* nested ring diagrams.

1. Introduction

The interest in discrete fluid models is rapidly increasing, the central topic being the investigation of the applicability of cellular automaton (CA) [1] fluid models for studying hydrodynamic phenomena [2]. In short, cellular automata are characterized by the discreteness in space and in time, which allows implementation on computers with relative ease. They evolve by means of updating rules. These rules in general do not represent fluid motion, but a subclass of these rules (then called collision rules) can be identified such that they reflect, for instance, conservation of particle number, momentum and/or energy. However, in most current models energy does not seem to be a quantity that can be properly defined to yield an independent conserved quantity. The most studied model in this field is the so-called FHP-model [2], named after Frisch, Hasslacher and Pomeau, with or without rest particles, the moving particles having unit speed in one of the six directions of an hexagonal lattice.

Relaxing the concept of momentum conservation (and thus the notion of sound-waves), a class of other well known models can be regarded as cellular automata, such as hopping diffusion, random walks on lattice with disorder [3, 4], and lattice versions of the clasical Lorentz gas [5]. In these models, the particles move independently of one another in an array of fixed scatterers/impurities.

Recently, we have considered a lattice Lorentz gas, with scatterers put at random on the sites of a square or (hyper)cubic lattice [6-8]. The collisions of the (mutually non-interacting) moving particles with these scatterers depend stochastically on the direction of the velocity of the incoming particles. The quantities of main interest are the response function, the velocity autocorrelation function (VACF) and the diffusion coefficient. Others have used deterministic collision rules (deflection angles) that are tied to the lattice [9, 10], mirror-like reflections [11] or deflections that depend on the parity of time [12]. For these Lorentz gases, the diffusion coefficient can easily be approximated using the molecular chaos assumption (Boltzmann appproximation). For the *stochastic* Lorentz gas, an analysis was performed that extends *beyond*

0305-4470/90/214953+24$03.50

Boltzmann [8], predicting values of the diffusion coefficient which agree very well with computer simulation data [6–8]. The success of this treatment is especially demonstrated in cases where the Boltzmann approximation *fails*, which occurs if the collision rules are such that backscattering of the moving particles at scatterers is possible. The method used is a generalization of the standard effective medium approximation (EMA) that has been applied successfully in the description of diffusion in bond percolation models [3, 13, 14]. In the standard EMA the system is described by a single effective rate constant; our generalized EMA contains in principle $b-1$ effective rate constants, where b is the coordination number of the lattice.

The stochastic Lorentz gas proves to be a model for which several approximations, that are standardly used in kinetic theory, can be evaluated explicitly; this in contrast to continuous models, where explicit calculations require great efforts, even on the level of the ring approximation [15, 16]. The latter will be defined later in the context of the present model. Calculations have been carried out for the hard-sphere gas [17] and the continuous Lorentz gas in two and three dimensions [18, 19]. Only for the latter, more complicated diagrams (than rings) were determined [19]. The simple lattice structure of the models allows explicit calculations to investigate the success and failure of these approximations in comparison with the effective medium approximation, as they work out for these models. This is the main objective of this paper. In addition to the Boltzmann approximation, the standard techniques we will discuss are the ring approximation, the repeated-ring approximation and their self-consistent formulations. Here, the term 'ring' is related to the return of the moving particle to a site it has already visited before, thus inducing correlations between collisions. The main result is that EMA gives a good approximation, although for instance orbiting particle trajectories [20] and general (Cayley-) tree-like trajectories are *not* accounted for. Very recently the low-density limit for the diffusion coefficient has been calculated *exactly* also for cases with reflections [21]. Then the dominant contributions come from trajectories on a Cayley-tree structure. In this paper we will show that EMA accounts for *all* ring and nested ring events. Although more complicated diagrams are not accounted for, the EMA results coincide, in the low-density limit, with the exact results.

The paper is organized as follows. In section 2 we give a description of the model and repeat some formalism needed from [8]. Then we consider fluctuation expansions in terms of free (empty lattice) propagators (section 3) and in terms of 'Boltzmann' propagators (section 4), the latter already having diffusive motion built in. In the remaining sections we discuss several approximations that collect the relevant terms from these fluctuation expansions. The Boltzmann approximation is given in section 6, and several ring approximations in sections 7 and 8. Next, in section 9, the effective medium approximation is formulated and the weights of the contributions are compared with that of a formally exact expansion. The details on weights are shifted in appendices. Finally, in section 10, numerical results are presented that show the breakdown of several of these approximations in comparison with EMA and simulation data.

2. Chapman–Kolmogorov equation and correlation functions

In this section we introduce the model by repeating some parts from [8] needed for a self-contained presentation. We consider a Lorentz gas on a d-dimensional cubic lattice [6, 8, 22] with N sites, denoted by $n=(n_1, n_2, \ldots, n_d)$, unit lattice distance and a fraction c of sites—chosen at random—occupied by scatterers. A particle moves with

unit speed from site to site. Its trajectories are straight lines until the particle hits a scatterer, where it will be scattered into one of the lattice directions with probabilities depending on the incident velocities.

Let $p(n, i, t)$ be the probability in a given configuration of scatterers that at the integer-valued time t the moving particle is at site n and arrives there with 'velocity' i (i.e. comes from lattice site $n - e_i$). Here velocity variables, denoted by labels $i, j, \ldots$ ($i, j = 1, 2, \ldots, 2d \bmod(2d)$), refer respectively to the lattice directions $e_1, e_2, \ldots, e_d$, $-e_1 (= e_{d+1}), -e_2, \ldots, -e_d$. We further use the convention that Greek labels ($\alpha, \beta = 1, 2, \ldots, d$) denote Cartesian components of d-vectors. The microscopic or fluctuating density of scatterers is described by the random variable c_n taking on the values

$$c_n = \begin{cases} 1 & \text{with probability } c \\ 0 & \text{with probability } 1 - c. \end{cases} \tag{2.1}$$

The distribution function for the moving particle is $\langle p(n, i, t) \rangle$, where $\langle \ldots \rangle$ denotes the quenched average over the configuration of scatterers, i.e. an average over all c_n with weight function (2.1).

The scattering laws are specified by introducing a transmission probability α, a reflection probability β and a deflection probability γ for any orthogonal direction, with normalization

$$\alpha + \beta + 2(d-1)\gamma = 1. \tag{2.2}$$

We write this in the form of a $2d \times 2d$ transition matrix

$$W_{ij} = \begin{pmatrix} \alpha & \gamma & \gamma & \cdot & \cdot & \cdot & \beta & \gamma & \gamma & \cdot & \cdot & \cdot \\ \gamma & \alpha & \gamma & \cdot & \cdot & \cdot & \gamma & \beta & \gamma & \cdot & \cdot & \cdot \\ \gamma & \gamma & \alpha & \cdot & \cdot & \cdot & \gamma & \gamma & \beta & \cdot & \cdot & \cdot \\ \cdot & \cdot & \cdot & \cdot & \cdot & \cdot & \cdot & \cdot & \cdot & \cdot & \cdot & \cdot \\ \cdot & \cdot & \cdot & \cdot & \cdot & \cdot & \cdot & \cdot & \cdot & \cdot & \cdot & \cdot \\ \beta & \gamma & \gamma & \cdot & \cdot & \cdot & \alpha & \gamma & \gamma & \cdot & \cdot & \cdot \\ \gamma & \beta & \gamma & \cdot & \cdot & \cdot & \gamma & \alpha & \gamma & \cdot & \cdot & \cdot \\ \gamma & \gamma & \beta & \cdot & \cdot & \cdot & \gamma & \gamma & \alpha & \cdot & \cdot & \cdot \\ \cdot & \cdot & \cdot & \cdot & \cdot & \cdot & \cdot & \cdot & \cdot & \cdot & \cdot & \cdot \\ \cdot & \cdot & \cdot & \cdot & \cdot & \cdot & \cdot & \cdot & \cdot & \cdot & \cdot & \cdot \end{pmatrix} \tag{2.3}$$

with $\Sigma_i W_{ij} = \Sigma_j W_{ij} = 1$. We shall also frequently use the $2d \times 2d$ velocity matrices V_α ($\alpha = 1, 2, \ldots, d$) which are diagonal matrices with components

$$(V_\alpha)_{ij} = \delta_{ij} e_{i\alpha} = \delta_{ij}(\delta_{i\alpha} - \delta_{i,\alpha+d}). \tag{2.4}$$

The Chapman-Kolmogorov equation for the probability distribution $p(n, i, t)$ in a given realization of scatterers is [23]:

$$p(n + e_i, i, t+1) = (1 - c_n)p(n, i, t) + c_n \sum_j W_{ij} p(n, j, t) \tag{2.5}$$

or in $(2dN \times 2dN)$-matrix form and $2dN$-vector notation:

$$p(t+1) = S^{-1}(1 + CT)p(t) \equiv (1 - L)p(t) \tag{2.6}$$

where S is the 'free streaming' operator

$$S_{ni,mj} = S_{nm}\delta_{ij} = \delta_{n+e_i,m}\delta_{ij} \tag{2.7}$$

C is the diagonal matrix of density fluctuations and $T = W - 1$ the collision operator, diagonal in the space variables:

$$C_{ni,mj} = c_n \delta_{nm} \delta_{ij} \tag{2.8}$$

$$T_{ni,mj} = \delta_{nm} W_{ij} - \delta_{nm} \delta_{ij} \tag{2.9}$$

and $L = 1 - S^{-1}(1 + CT)$ is the stochastic Liouville operator. Equation (2.6) has the formal solution for $t \geqslant 1$ [8]:

$$p(t) = [S^{-1}(1 + CT)]^{t-1} S^{-1} p(0) = (1 - L)^{t-1} S^{-1} p(0). \tag{2.10}$$

Henceforth, we will only indicate the explicit space and/or velocity dependence if clarity requires such. Equation (2.6) applies to the conditional probability $P(t)$, with initial condition $P(0) = 1$ or $P_{ni,mj}(0) = \delta_{nm} \delta_{ij}$.

Next, a vector notation is introduced which decomposes the $2d$-dimensional velocity space into the eigenspaces of a general cubic symmetric matrix, i.e. a matrix of the form (2.3), without constraint (2.2). The simultaneous eigenvectors of these matrices are $|1\rangle$ with components $|1\rangle_i = 1$ and $i = 1, 2, \ldots, 2d$, $|V_\alpha\rangle = V_\alpha |1\rangle$ and $|dV_\alpha^2 - 1\rangle = (dV_\alpha^2 - 1)|1\rangle$ with $\alpha = 1, 2, \ldots, d$. Its eigenvalues are $\alpha + \beta + 2(d-1)\gamma$, $\alpha - \beta$ and $\alpha + \beta - 2\gamma$, respectively, having multiplicity 1, d and $d - 1$, respectively. Their diagonalizability implies that the cubic symmetric matrices commute. The inner product is defined as

$$\langle a(V) | b(V) \rangle = \frac{1}{2d} \sum_i a(e_i) b(e_i). \tag{2.11}$$

For details we refer to [8].

The quantities of interest are the response function, the velocity autocorrelation function and the diffusion coefficient. They can all be expressed in terms of the two time probability distribution p in the steady state or in terms of the matrix of conditional probabilties P and a uniform initial distribution $(2dN)^{-1}$, related by:

$$\langle p(n, i, t; m, j, 0) \rangle = \frac{1}{2dN} \langle P_{ni,mj}(t) \rangle. \tag{2.12}$$

We obtain the propagator from this by a Laplace transform, which, for discrete times, is conveniently written as

$$\begin{aligned} \Gamma(z) &= \sum_{t=1}^{\infty} (1+z)^{-t} \langle P(t) \rangle = \langle (z + L)^{-1} S^{-1} \rangle \\ &= \langle [(1+z)S - 1 - CT]^{-1} \rangle. \end{aligned} \tag{2.13}$$

The dynamic structure function or response function $\mathcal{F}(q, z)$ is the Fourier-Laplace transform of the probability for a displacement $(n - m)$:

$$\mathcal{F}(q, z) = \langle 1 | \hat{\Gamma}(q, z) | 1 \rangle = \frac{1}{2d} \sum_{ij} \langle \hat{\Gamma}_{ij}(q, z) \rangle \tag{2.14}$$

and the Laplace transform of the VACF becomes

$$\Phi(z) = \frac{1}{d} \sum_\alpha \langle V_\alpha | \hat{\Gamma}(0, z) | V_\alpha \rangle = \frac{1}{2d^2} \sum_\alpha \sum_{ij} e_{i\alpha} \langle \hat{\Gamma}_{ij}(0, z) \rangle e_{j\alpha}. \tag{2.15}$$

To obtain the diffusion coefficient

$$D = \Phi(0) - \frac{1}{2d} \tag{2.16}$$

one has to evaluate the VACF at $z = 0$ [8].

The Fourier transform of a matrix $A_{ni,mj}$ is defined as

$$\hat{A}_{ij}(q, q') = \frac{1}{N} \sum_{n,m} e^{-iqn} A_{ni,mj} e^{iq'm}. \tag{2.17}$$

For a translationally invariant matrix A, i.e. depending only on $(n-m)$, the Fourier transform is diagonal with elements

$$\hat{A}_{ij}(q) = \sum_{n} e^{-iqn} A_{ni,0j} \tag{2.18}$$

and inverse transformation

$$A_{ni,mj} = \frac{1}{N} \sum_{q \in 1BZ} e^{iqn} \hat{A}_{ij}(q) \equiv \int_{q} e^{iqn} \hat{A}_{ij}(q). \tag{2.19}$$

The q are reciprocal lattice vectors, located in the first Brillouin zone (1BZ) of the hypercubic lattice. In the thermodynamic limit, where the number of lattice sites n becomes large, the q-sum may be replaced by an integral, and the integration ymbol stands for

$$\int_{q} (\ldots) = \int_{-\pi}^{\pi} \ldots \int_{-\pi}^{\pi} \frac{d^{(d)}q}{(2\pi)^d} (\ldots). \tag{2.20}$$

In [8] we evaluated the diffusion coefficient D, in some approximations of the propagator (2.13). The most drastic approximation is to assume molecular chaos (Boltzmann approximation) and replace the random matrix C in (2.13) by its average $\langle C \rangle = c\mathbf{1}$. This is equivalent to replacing the Lorentz gas on a quenched random lattice by a type of random walk on a uniform lattice with average transition rates [25]. A more sophisticated approximation, developed in [8], is the so-called effective medium approximation (EMA). It is obtained by imposing that the first order correction to a resummation of this Boltzmann propagator be vanishing. This yields a self-consistent relation for the eigenvalues of the effective collision operator T^e.

The goal of this paper is to present a systematic analysis and a discussion of the standard approximations, used in kinetic theory, such as the Boltzmann equation and the ring equations. We will compare the contributions accounted for by the different approximations. We will do this in the context of fluctuation expansions, involving free propagators, Boltzmann propagators or effective medium propagators, respectively.

3. Free propagators

The matrix elements $\Gamma_{nm}(z)$ of the propagator (2.13) of the moving particle, averaged over fixed configurations of scatterers, may be expanded in collision sequences. In order to do so, we denote the propagator of the empty lattice (all $c_n = 0$) by $\Gamma^f = ((1+z)S - 1)^{-1}$ and call this the *free particle propagator.* Note that by translational symmetry $\Gamma_{nm}(z)$ and $\Gamma^f_{nm}(z)$ depend only on $(n-m)$. The resolvent operator in (2.13), with L defined in (2.10) is expanded as:

$$(z+L)^{-1}S^{-1} = \Gamma^f + \Gamma^f C T \Gamma^f + \Gamma^f C T \Gamma^f C T \Gamma^f + \ldots. \tag{3.1}$$

Here, $(CT)_{nm} = c_n T\delta_{nm}$ is diagonal and c_n indicates the presence ($c_n = 1$) or absence ($c_n = 0$) of a scatterer at site n. The intermediate sums in (3.1) over scatterers involve factors $c_n c_{n_1} c_{n_2}, \ldots$, where $n, n_1, n_2, \ldots$, run over the whole lattice and thus may refer to the same or to different positions of scatterers. These products of c are the weights for the terms in the expansion. The quenched average in (3.1) then corresponds to the average of these weight factors, in which we have to account for correlations between the c_n in the above sequence. Let $l, l_1, l_2, \ldots$, be the number of occurrences of the scatterers at respectively $n, n_1, n_2, \ldots$, in a given term in the expansion (3.1), then the weight factor is

$$\langle c_n c_{n_1} c_{n_2} \ldots \rangle = \langle c_n^l c_{n_1}^{l_1} c_{n_2}^{l_2} \ldots \rangle = \mu_l^0 \mu_{l_1}^0 \mu_{l_2}^0 \ldots \mu_{l_{k-1}}^0 = c^k \tag{3.2}$$

where k is the number of *different* scatterers involved. Here we used the moments μ_l^0 of the distribution of c_n: $\mu_l^0 \equiv \langle c_n^l \rangle = \langle c_n \rangle = c$. Thus, a weight factor c^k is assigned to each term in a multiple sum in (3.1) that involves k diffeent scatterers. The formal expansion of the propagator Γ in (2.13) can now be written as

$$\Gamma_{n0} = \Gamma^f_{n0} + c \sum_m \Gamma^f_{nm} T \Gamma^f_{m0} + c^2 \sum_{m \neq m'} \Gamma^f_{nm} T \Gamma^f_{mm'} T \Gamma^f_{m'0} + c \sum_m \Gamma^f_{nm} T \Gamma^f_{00} T \Gamma^f_{m0} + \ldots \tag{3.3}$$

where the relation $\Gamma_{mm} = \Gamma_{00}$ has been used. The individual terms in this series can be represented by diagrams (see figure 1). The solid lines represent free propagators Γ^f and dots represent T-vertices. Dots referring to the same scatterer are connected by arcs. The first line on the RHS of figure 1 represents the terms written explicitly in (3.3). The last term in (3.3)—and similar terms in figure 1—representing two subsequent collisions of the moving particle with the same scatterer and with only intermediate free streaming are vanishing of course, as at least one other scatterer is needed for the particle to return to the first scatterer.

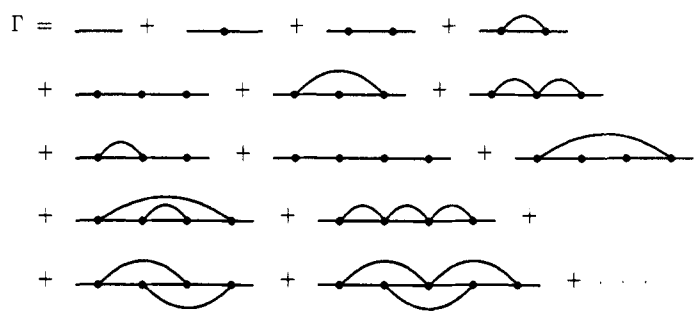

Figure 1. Diagrammatic expansion of exact propagator Γ in free propagators (——) and T-vertices (●), see equation (3.1). Only some typical low-order diagrams are shown.

Because the restricted sums no longer represent matrix products, we want to eliminate the constraints. This will yield new weight factors for the diagrams. As an illustration, consider the RHS of the expansion (3.3), where we add the term with $m = m'$ to the third term and subtract it from the fourth one (as it is of the same structure as all the terms in this summation). This forces us to change the weight of the fourth term from c to $\kappa_2^0 \equiv c - c^2$. Thus, if a scatterer occurs twice, the corresponding weight is κ_2^0, and if a scatterer occurs j times, its weight is κ_j^0. A constructive proof of this is given in appendix A. In general the *new weight factor* for a diagram with

unconstrained sums is $\Pi_{j=1}^{\infty}(\kappa_j^0)^{l_j}$ if the diagram has l_j $(j=1,2,\ldots)$ sets of j connected vertices [26]. Here κ_j^0 are the cumulants corresponding to the moments $\mu_l^0=\langle c_n^l\rangle=c$. From the generating functions for the moments and cumulants:

$$F^0(x)=\sum_{l=0}^{\infty}\mu_l^0\frac{x^l}{l!}=1+c(e^x-1)$$
$$C^0(x)\equiv\log F^0(x)=\sum_{l=0}^{\infty}\kappa_l^0\frac{x^l}{l!}=\log(1+c(e^x-1)) \tag{3.4}$$

one obtains the expressions for κ_l^0, where we defined $\mu_0^0\equiv 1$. An explicit calculation is given in appendix B. As an illustration we quote the weights of the diagrams in figure 1. They are 1, κ_1^0, $(\kappa_1^0)^2$, κ_2^0, $(\kappa_1^0)^3$, $\kappa_1^0\kappa_2^0$, κ_3^0, $\kappa_2^0\kappa_1^0$, $(\kappa_1^0)^4$, $(\kappa_1^0)^2\kappa_2^0$, $(\kappa_2^0)^2$, κ_4^0, $(\kappa_2^0)^2$, and $\kappa_2^0\kappa_3^0$, respectively. We stress that the relation with these cumulants was known before only for the first few terms [26]. Appendix A contains a general proof that the weights are indeed the cumulants of the probability distribution (2.1).

In standard nomenclature the diagrams #2, 3, 5, 9, ..., in figure 1 represent *uncorrelated collisions*; diagrams #4, 6, 8, 10, ..., *simple ring collisions*; diagrams #7, 12, ..., *repeated ring collisions* and diagrams like #11 *nested ring collisions* (rings within rings). The last line of figure 1 shows two more complicated non-ring diagrams (diagrams #13 and #14).

As a motivation of the approximations to be discussed later, we note that the various apprximations in kinetic theory are based on various resummations of subsets of diagrams. To select these subsets, we have to estimate the magnitude or phase space of different diagrams at small concentration of scatterers, c, and at large times, where t is typically on the order of the mean free time $t_{mf}=1/c$. In a *systematic* resummation scheme one selects out of the whole set of $\mathcal{O}(c^k)$-diagrams all those that are most divergent as $t\to\infty$, and sum over k. In this sense, most resummations considered here are not systematic.

Instead of calculating in detail some of the terms in the expansion in free propagators, which has not been done yet, we will just give some phase space estimates for the various collision sequences that can occur (see figure 2). The method is the same as was used by Hauge and Cohen [20].

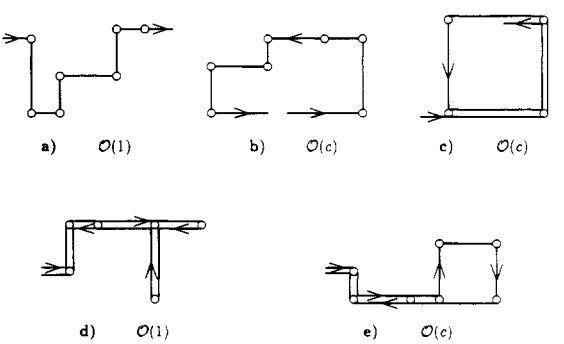

Figure 2. Comparison of phase space for some typical particle trajectories. (*a*) uncorrelated collisions, (*b*) ring collision, (*c*) orbiting collision sequence, (*d*) nested (repeated) ring with backscattering ($\beta\neq 0$) and (*e*) nested ring without backscattering.

In the case of uncorrelated collisions, which are accounted for in the Boltzmann approximation, the phase space for k uncorrelated collisions is proportional to $(ct)^k \sim \mathcal{O}(1)$, with $t \sim t_{\mathrm{mf}}$, see figure 2(a). In a similar fashion one estimates the phase space of ring collisions to be $c(ct)^{k-1} \sim \mathcal{O}(c)$ (see figure 2(b), where the last vertical motion of the moving particle has a length that is fixed by the first one, in order to be on the same horizontal line after the collision; consequently this piece does not add a factor $t \sim t_{\mathrm{mf}} = 1/c$.) For orbiting collisions [20] (see figure 2(c)) the same argument applies. For models *with backscattering* ($\beta \neq 0$) there exist purely retracing 'nested' (repeated) ring collisions (see figure 2(d)), which have the *same* phase space as the uncorrelated collisions. For cases *without backscattering* retracing events have typically a ring at the end (see figure 2(e)), thus yielding $c(ct)^{k-1} \sim \mathcal{O}(c)$.

These estimates clearly show that for cases with backscattering it will not be sufficient to resum only uncorrelated collisions (as will be the case in the Boltzmann equation), since there are correlated collisions (see for instance figure 2(d)) that have the same phase space. These estimates motivate the approximations constructed in the following sections.

4. Boltzmann propagators

The free propagators described in section 3 correspond to straight line motion and do not exhibit any diffusive behavior. To obtain diffusive behavior the particle has to suffer collisions. This can be achieved by including partial resummations of the terms on the RHS of (3.3). In the standard case the uncorrelated collisions constitute the complete set of most divergent diagrams for $c \to 0$ and $t \to \infty$, such that $ct \sim$ const. A standard procedure to remove the most† divergent long-time behaviour of the propagators at low densities is to introduce Boltzmann propagators G^0, by resumming only uncorrelated collisions in the expansion (3.1). This is exact for short times, where the moving particle has not yet had the possibility to hit the same scatterer twice. (For instance, in absence of reflections this is the case up to four time steps.) The resummation is carried out by replacing every occurrence of the random matrix C by its average, being c times the unity matrix. The Boltzmann propagator G^0 is then obtained by summing all these contributions from uncorrelated collisions, shortly written as

$$G^0 = \Gamma^f + \Gamma^f c T G^0 \tag{4.1}$$

or

$$G^0 = [\Gamma^{f^{-1}} - cT]^{-1} = [(1+z)S - 1 - cT]^{-1}. \tag{4.2}$$

The formal expansion of the resolvent operator in (3.1) in terms of these Boltzmann propagators is obtained from (4.1) and (4.2) by replacing Γ^f by G^0 and cT by $(C-c)T$. This leads to an expansion of the propagator Γ in G^0, where c_n in (3.1), (3.2) and (3.3) is replaced by $\delta c_n \equiv c_n - c$. The analog of free propagation in (3.1) ($c_n = 0$) is now propagation involving only uncorrelated collisions (Boltzmann propagation: $\delta c_n = 0$ or $c_n = c$). The vertices accounted for explicitly ($c_n = 1$ in (3.1)) now have the weights $(1-c)$ or $(-c)$ for $c_n = 1$ or $c_n = 0$, respectively. The moments μ_l^0 of the c_n are replaced by the central moments $\mu_l = \langle (\delta c_n)^l \rangle = \langle (c_n - c)^l \rangle$, yielding the expansions in Boltzmann

† As we shall see later on, in LGCAs there exist correlated collision diagrams which are as divergent as the uncorrelated ones.

propagators

$$\begin{aligned}\Gamma_{n0} = G^0_{n0} &+ \mu_2 \sum_{n_1} G^0_{nn_1} TG^0_{00} TG^0_{n_1 0} + \mu_3 \sum_{n_1} G^0_{nn_1} TG^0_{00} TG^0_{00} TG^0_{n_1 0} \\ &+ \mu_4 \sum_{n_1} G^0_{nn_1} TG^0_{00} TG^0_{00} TG^0_{00} TG^0_{n_1 0} \\ &+ \mu_2^2 \sum_{n_1 \neq n_2} G^0_{nn_1} TG^0_{00} TG^0_{n_1 n_2} TG^0_{00} TG^0_{n_2 0} \\ &+ \mu_2^2 \sum_{n_1 \neq n_2} G^0_{nn_1} TG^0_{n_1 n_2} TG^0_{00} TG^0_{n_2 n_1} TG^0_{n_1 0} \\ &+ \mu_2^2 \sum_{n_1 \neq n_2} G^0_{nn_1} TG^0_{n_1 n_2} TG^0_{n_2 n_1} TG^0_{n_1 n_2} TG^0_{n_2 0} + \ldots . \end{aligned} \tag{4.3}$$

Note that the analogues of the second and third term in the expansion (3.3) are vanishing here, because $\mu_1 = \langle \delta c_n \rangle = 0$. Finally, the constraints on the summations are eliminated by replacing the μ_l in (4.3) by the cumulants κ_l (see appendix A). The μ_l and κ_l are defined through their generating functions:

$$\begin{aligned} F(x) &= \sum_{l=0}^{\infty} \mu_l \frac{x^l}{l!} = \langle e^{(c_n - c)x} \rangle = e^{-cx} F^0(x) \\ C(x) &\equiv \log F(x) = \sum_{l=0}^{\infty} \kappa_l \frac{x^l}{l!} = -cx + C^0(x). \end{aligned} \tag{4.4}$$

The cumulants κ_l and κ_l^0 can be expressed in terms of moments as well as in terms of the concentration c, as will be explained in appendix B. Here we only note that $\kappa_l = \kappa_l^0 (l \geqslant 2)$ and $\kappa_1 = \mu_1 = 0$ and $\kappa_2 = \mu_2 = c(1-c)$.

We return to the expansion of the exact propagator in terms of Boltzmann propagators G^0 (compare (3.1)). Isolated T-vertices do not occur in the Boltzmann expansion, because $\kappa_1 = \mu_1 = 0$, and the new weight factor for a diagram is $\Pi_{j=2}^{l} (\kappa_j)^{l_j}$. The exact propagator in terms of Boltzmann propagators is diagrammatically shown in figure 3; in terms of unconstraint sums (see appendix A) it is explicitly written as:

$$\begin{aligned}\Gamma_{n0} = G^0_{n0} &+ \kappa_2 \sum_{n_1} G^0_{nn_1} TG^0_{00} TG^0_{n_1 0} + \kappa_3 \sum_{n_1} G^0_{nn_1} TG^0_{00} TG^0_{00} TG^0_{n_1 0} \\ &+ \kappa_4 \sum_{n_1} G^0_{nn_1} TG^0_{00} TG^0_{00} TG^0_{00} TG^0_{n_1 0} \\ &+ \kappa_2^2 \sum_{n_1 n_2} G^0_{nn_1} TG^0_{00} TG^0_{n_1 n_2} TG^0_{00} TG^0_{n_2 0} \\ &+ \kappa_2^2 \sum_{n_1 n_2} G^0_{nn_1} TG^0_{n_1 n_2} TG^0_{00} TG^0_{n_2 n_1} TG^0_{n_1 0} \\ &+ \kappa_2^2 \sum_{n_1 n_2} G^0_{nn_1} TG^0_{n_1 n_2} TG^0_{n_2 n_1} TG^0_{n_1 n_2} TG^0_{n_2 0} + \ldots . \end{aligned} \tag{4.5}$$

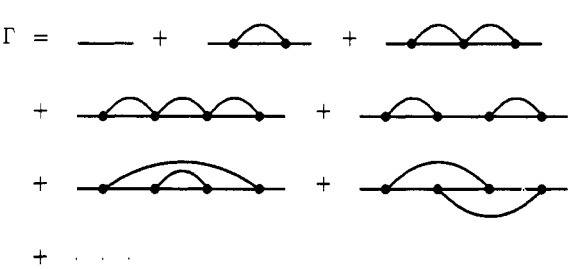

Figure 3. Diagrammatic expansion of exact propagator Γ in uncorrelated collision propagators G^0 (——) and collision operator fluctuations $\delta T = \delta c_n T$ (●), see equation (4.3). All terms up to fourth order are shown.

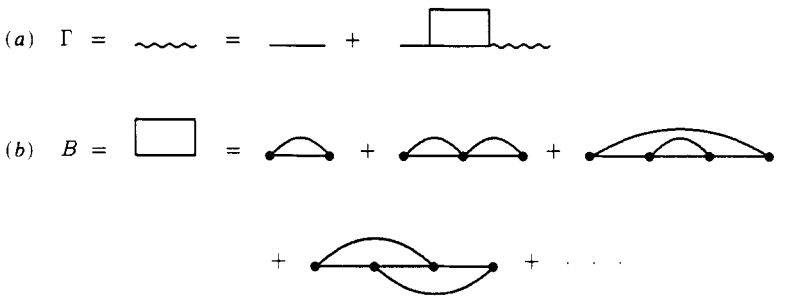

Figure 4. Dyson equation (4.6) in diagrammatic form (a) with collision (self-energy) diagrams (b).

Translational symmetry has been used in $G^0_{nn} = G^0_{00}$ and in the expressions inside brackets. We summarize equation (4.5) in the form of a Dyson equation:

$$\Gamma = G^0 + G^0 B \Gamma = [G^{0-1} - B]^{-1} \tag{4.6}$$

or diagrammatically in figure 4. B denotes the set of collision (self-energy) diagrams beyond the Boltzmann or uncorrelated collision diagrams, see figure 4(b). In Fourier representation the single particle propagator becomes

$$\hat{\Gamma}(q, z) = [(1+z)\, e^{iqV} - 1 - cT - \hat{B}(q, z)]^{-1} \tag{4.7}$$

and the Laplace transform of the VACF is, on account of (2.15),

$$\Phi(z) = \frac{1}{d} \sum_{\alpha} \langle V_\alpha | [z - cT - \hat{B}(0, z)]^{-1} | V_\alpha \rangle. \tag{4.8}$$

We note that the q-independent matrix $\hat{B}(0, z)$ also has the cubic symmetric form (2.3). So its eigenvectors are known and also the relation between their eigenvalues and the elements of the matrix $\hat{B}(0, z)$ (see discussion below (2.10)). Consequently, the above equation can be written in terms of eigenvalues as

$$\Phi(z) = \frac{1}{d} \frac{1}{z - ct_\upsilon - b_\upsilon(z)} \tag{4.9}$$

where $b_\upsilon(z)$ is the eigenvalue of $\hat{B}(0, z)$ corresponding with $|V_\alpha\rangle$.

5. Approximate kinetic equations

In absence of exact results for the formal solution (2.10) of the Liouville equation, or its expansion in free propagators or Boltzmann propagators, an approximate method can be followed to calculate some quantities of interest, e.g., diffusion coefficient or velocity autocorrelation function (2.15). In the remaining part of this paper we describe the standard approximations in the context of the present model. We start with some guiding remarks concerning the methods.

An obvious approximation is to assume molecular chaos (Boltzmann approximation), i.e. neglecting correlations between collisions. As there is no interaction between moving particles, these correlations necessarily correspond to visits of a moving particle

to a scatterer it has already hit before; of course correlations occur also in case the revisited site is empty, and we have so-called 'virtual' collisions. The return to a site is usually called a *ring event*, that is, if all intermediate collisions are uncorrelated. All approximations to be discussed here, going *beyond* Boltzmann, involve *ring* integrals; they are the ring approximation (RA), repeated-ring approximation (RRA), self-consistent ring approximation (SRA), self-consistent repeated-ring approximation (SRRA) and finally the effective medium approximation, as developed in [8]. Events *not* accounted for are diagrams referring, for instance, to crossings between different scatterers, such as the last explicitly written terms in (4.3) (cf. figure 3) or the last line of figure 1. Evaluation of such (non-ring) diagrams would involve (multiple) sums over the lattice (a subclass of which was calculated for the bond percolation model [27-29]). Ring diagrams do not exhibit these technical difficulties.

6. Boltzmann approximation

This approximation accounts for all uncorrelated collisions. For cases without backscattering ($\beta = 0$) it is expected to give the correct low-density behaviour, as we have argued with the help of figure 2. These phase space estimates show that the most divergent diagrams for $c \to 0$, $t \to \infty$ with $ct = \text{const}$ are the uncorrelated collisions of figure 2(a), because the retracing nested rings of $\mathcal{O}(1)$ (see figure 2(d)) are absent. The uncorrelated collision sequences are the diagrams in (3.1) with isolated T-vertices. They have been summed to give the Boltzmann propagator (4.2). The higher order collision operator in (4.6) vanishes in this approximation: $B^0 = 0$. The Fourier transform of the single particle propagator becomes then

$$\hat{\Gamma}^0(q, z) \equiv \hat{G}^0(q, z) = [(1+z)\,\mathrm{e}^{\mathrm{i}qV} - 1 - cT]^{-1} \tag{6.1}$$

where $\hat{S}(q) = \exp(\mathrm{i}qV)$ is the Fourier transform (2.18) of the translational invariant free streaming operator (2.7). The diffusion coefficient is given by (2.16) with the VACF given by (4.8) which can be calculated in a straightforward manner. In fact the model is approximated by a uniform lattice with modified transition probabilities $\alpha' = 1 - c(1-\alpha)$, $\beta' = c\beta$ and $\gamma' = c\gamma$ and the diffusion coefficient is [4, 8, 24, 25, 30]:

$$D = \frac{1}{d(1-\alpha'+\beta')} - \frac{1}{2d} = \frac{1}{dc(1-\alpha+\beta)} - \frac{1}{2d} \tag{6.2}$$

where d is the number of space dimensions. For the completely filled lattice ($c = 1$) the Boltzmann approximation is exact, as there is no disorder to yield correlation effects. Recall that in the limit $c \to 0$ the Boltzmann approximation is only exact for cases *without* backscattering, i.e. $\beta = 0$.

7. Ring and repeated-ring approximation

In the next approximation ring events will be taken into account. For models without reflection this will affect the $O(c)$ contribution, while for the models with reflection inclusion of ring terms is expected to modify even the $\mathcal{O}(1)$ term in the low-density expansion. The ring diagram (the simplest diagram that involves correlation between

collisions) is the first term on the RHS of figure 4(*b*). Replacing the weight $\kappa_2(=c(1-c))$ by its low- or high-density approximation, we define the *ring approximation* by

$$B_{RA} = cTR^0T \quad \text{for small } c$$
$$B_{RA} = pTR^0T \quad \text{for small } p = 1-c \tag{7.1}$$

where R^0 is the *simple ring* integral

$$R^0(z) \equiv G^0_{00} = \int_q \hat{G}^0(q, z) = \int_q [(1+z)\,e^{iqV} - 1 - cT]^{-1}. \tag{7.2}$$

The matrix $R^0(z) = G^0_{00}(z)$ represents in this approximation the Laplace transform of the matrix of conditional probabilities $\langle P_{00}(t)\rangle$ to find the particle at the origin given that it started at the origin at $t = 0$. The ring kinetic equations for low and high densities are then expressed by the propagators

$$\hat{\Gamma}_{RA}(q, z) = [(1+z)\,e^{iqV} - 1 - cT - cTR^0(z)T]^{-1} \tag{7.3}$$

and

$$\hat{\Gamma}_{RA}(q, z) = [(1+z)\,e^{iqV} - 1 - T + pT - pTR^0(z)T]^{-1} \tag{7.4}$$

respectively. Note that according to this approximation the particle is moving, between subsequent returns to the origin, in a 'modified' Boltzmann background which, however, depends on the Laplace variable z. Observe again that T, R^0 and B_{RA} are (commuting) cubic symmetric matrices.

The ring approximation thus requires calculation of the ring integral over the Boltzmann propagator (6.1). Instead of calculating the full integral, using a decomposition into eigenspaces of the collision term cT, one can also evaluate explicit contributions to the ring integral for some specific particle trajectories. This can be done by expanding the integrand in (7.3) or (7.4) in powers of real and virtual collision matrices, being the diagonal and off-diagonal part of T, respectively. However, we have not carried this out.

Next we consider the *repeated-ring approximation.* Here one takes into account all events with multiple returns of the moving particle to the same site, i.e. the first and second term and analogous higher order terms on the RHS of figure 4(*b*). The weight factors κ_l are replaced by their low- or high-density value (B8). The cubic symmetric collision operators are then

$$B_{RRA} = cTR^0T + cT(R^0T)^2 + cT(R^0T)^3 + \ldots = cTR^0T(1 - R^0T)^{-1} \tag{7.5}$$

and

$$B_{RRA} = pTR^0T - pT(R^0T)^2 + pT(R^0T)^3 + \ldots = pTR^0T(1 + R^0T)^{-1} \tag{7.6}$$

respectively, and the propagators are, on account of (4.7):

$$\hat{\Gamma}_{RRA}(q, z) = [(1+z)\,e^{iqV} - 1 - cT(1 - R^0(z)T)^{-1}]^{-1} \tag{7.7}$$

and

$$\hat{\Gamma}_{RRA}(q, z) = [(1+z)\,e^{iqV} - 1 - T + pT(1 + R^0(z)T)^{-1}]^{-1}. \tag{7.8}$$

8. Self-consistent ring approximations

The self-consistent ring approximation resembles the ring approximation (7.3). It is, however, quite different in the sense that the cubic symmetric collision operator

$$B_{\mathrm{SRA}} = cTRT \tag{8.1}$$

and the ring operator R are obtained from

$$R(z) = G_{00}(z) = \int_q \hat{G}(q, z) \tag{8.2}$$

(compare (7.2)) where the propagator $\hat{G}$ depends itself on R in a *self-consistent* manner:

$$\hat{\Gamma}_{\mathrm{SRA}}(q, z) = \hat{G}(q, z) = [(1+z)\,\mathrm{e}^{\mathrm{i}qV} - 1 - cT - cTR(z)T]^{-1}. \tag{8.3}$$

Iteration of the equations (8.2) and (8.3) yields the nested ring diagrams (rings within rings). The high-density limit is treated analogously.

Obviously, the repeated-ring approximation can be given the same treatment. Here the collision operator $T + TRT$ in (8.3) is replaced by repeated rings; consequently

$$B_{\mathrm{RRA}} = cTRT + cTRTRT + \ldots = cTRT(1 - RT)^{-1} \tag{8.4}$$

where the weights κ_l are again approximated by their low-density values: $\kappa_l \sim c$.

The self-consistent ring integral (8.2) is again defined in terms of the complete propagator, now being

$$\hat{\Gamma}_{\mathrm{SRRA}}(q, z) = \hat{G}(q, z) = [(1+z)\,\mathrm{e}^{\mathrm{i}qV} - 1 - cT(1 - R(z)T)^{-1}]^{-1}. \tag{8.5}$$

And similarly for the high-density case. The self-consistent repeated-ring approximation is then obtained by iteration of (8.2) and (8.5). This yields nested repeated and repeated nested ring diagrams, henceforth referred to as *nested rings*. Each diagram obtains the weight c^k, where k is the number of different scatterers involved in the diagram. At this point it may be instructive to write out some iteration steps explicitly in diagrammatic form. For this we refer to figure 5.

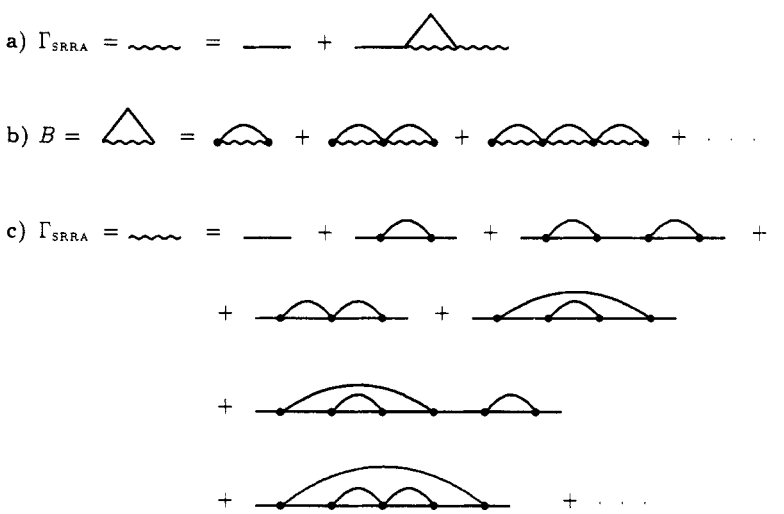

Figure 5. Self-consistent repeated-ring (SRRA) equation (*a*), with collision diagrams (*b*). (*c*) iteration of (*a*) and (*b*).

9. Effective medium approximation (EMA)

The effective medium approximation has been applied successfully in the past to the problem of hopping models, random resistor networks and bond percolation models. One way to derive this is to assume effective transition rates for every link except one, which is treated exactly [31]. Another, equivalent, method is to consider a fluctuation expansion around an effective medium, which is defined in a self-consistent manner by imposing that the first order perturbation be zero [13, 14]. The EMA equation resulting from these operations qualitatively describes the diffusion coefficient and velocity autocorrelation function in the above classes of models [14]. For the present model, the EMA is generalized to three effective transition rates, instead of one, satisfying the normalization (2.2). The details are given in [8] Here we formulate it in a way that allows transparent comparison with the approximations discussed in the preceding sections.

We introduce an EMA propagator

$$\hat{\Gamma}_{\mathrm{EMA}}(q, z) = \hat{G}(q, z) = [(1+z)\,\mathrm{e}^{\mathrm{i}qV} - 1 - cT^{\mathrm{e}}(z)]^{-1} \tag{9.1}$$

where $cT + B$ in (4.7) is replaced by an effective (as yet unknown) collision operator $T^{\mathrm{e}}(z)$. Then we formally expand the exact propagator (2.13) in powers of δT_n, defined as $\delta T_n \equiv c_n T - cT^{\mathrm{e}}$, and resum all repeated visits of the moving particle to the same scatterer. This is achieved by replacing δT_n by $\Theta_n = \delta T_n (1 - R\delta T_n)^{-1}$ with $R(z) = G_{00}(z)$ and by imposing that consecutive intermediate site labels are different. The result is

$$\Gamma_{n0} = G_{n0} + \sum_{n_1} G_{nn_1}\langle\Theta_{n_1}\rangle G_{n_1 0} + \sum_{n_1 \neq n_2} G_{nn_1}\langle\Theta_{n_1}\rangle G_{n_1 n_2}\langle\Theta_{n_2}\rangle G_{n_2 0}$$
$$+ \sum_{n_1 \neq n_2} \langle G_{nn_1}\Theta_{n_1} G_{n_1 n_2}\Theta_{n_2} G_{n_2 n_1}\Theta_{n_1} G_{n_1 n_2}\Theta_{n_2} G_{n_2 0}\rangle + \ldots . \tag{9.2}$$

The essential step [13, 14] in the EMA is to choose $T^{\mathrm{e}}(z)$ such that $\langle\Theta_n\rangle = 0$ (EMA condition) and neglect all higher-order terms in Θ_n. Just because of the EMA condition, non-vanishing higher-order terms are at least fourth order (last line in (9.2)). Hence the EMA propagator is given by (9.1), where $T^{\mathrm{e}}(z)$ is determined in a self-consistent manner from the EMA condition $\langle\Theta_n\rangle = 0$. Writing out this average with the help of $\langle f(c_n)\rangle = cf(1) + (1-c)f(0)$ yields, after some rearrangements, the EMA condition:

$$\frac{c}{1-(T-cT^{\mathrm{e}})R}[T - T^{\mathrm{e}} + TRT^{\mathrm{e}} - cT^{\mathrm{e}}RT^{\mathrm{e}}]\frac{1}{1+cRT^{\mathrm{e}}} = 0 \tag{9.3}$$

or

$$T^{\mathrm{e}} = T + TRT^{\mathrm{e}} - cT^{\mathrm{e}}RT^{\mathrm{e}} \tag{9.4}$$

where $T^{\mathrm{e}} = T^{\mathrm{e}}(z)$ and $R = R(z)$. Here $R(z)$ is given through (8.2) where $\hat{G}$ is the EMA propagator (9.1). T, $T^{\mathrm{e}}(z)$ and $R(z)$ are again commuting cubic symmetric matrices. A closer look at (9.4) shows that the EMA equation 'contains' the approximation schemes defined in the preceding sections. For, if we restrict ourselves to leading order in c, i.e. neglecting the last term, we can iterate $T^{\mathrm{e}} = T + TRT^{\mathrm{e}}$, yielding repeated rings. With self-consistent evaluation of the ring matrix, one obtains the self-consistent repeated-ring equation. A further restriction to $T^{\mathrm{e}} = T + TRT$ gives the ring and self-consistent ring equation, respectively. Also for the high-density limit (9.4) can be shown to recover the repeated-ring collision operator.

In terms of the collision operator (figure 4(*b*)) we have $B_{\mathrm{EMA}} = cT^{\mathrm{e}} - cT$. Iteration of (9.4) yields an expansion of T^{e} in powers of RT, very similar to the SSR approximation in (8.4):

$$cT^{\mathrm{e}} = \sum_{l=1}^{\infty} \nu_l T(RT)^{l-1}. \tag{9.5}$$

The essential difference, however, is the occurrence of different weights ν_l, where the SRRA has the same weight c for every term in the sum. The ν_l are also different from the κ_l of the exact expansion (4.5). In the sequel, we will consider these coefficients in more detail, investigating their origin and comparing them with the exact coefficients κ_l. The first few coefficients are given by

$$\begin{aligned} &\nu_1 = c \qquad \nu_2 = c(1-c) \qquad \nu_3 = c(1-c)(1-2c) \\ &\nu_4 = c - 6c^2 + 10c^3 - 5c^4. \end{aligned} \tag{9.6}$$

Note that ν_1, ν_2 and ν_3 are equal to κ_1^0, $\kappa_2 = \kappa_2^0$ and $\kappa_3 = \kappa_3^0$, respectively, but all higher-order ν_l are different from the corresponding κ_l. Note also that $\nu_1 \neq \kappa_1 = 0$; this is explained by the fact that the κ refer to the 'self-energy' diagrams B in $cT^{\mathrm{e}} = cT + B$, while ν_1 accounts for the first term cT. The generating function $A(x)$ of these coefficients is easily obtained by renaming $RT = x$ and $cRT^{\mathrm{e}} = A(x)$. Then, multiplying (9.5) by c yields

$$A(x) = \sum_{l=1} \nu_l x^l \tag{9.7}$$

where $A(x)$ satisfies $A = cx + xA - A^2$, as follows from (9.4). The solution of this equation with boundary condition $A = 0$ for $c = 0$ is:

$$A(x) = \tfrac{1}{2}\{-1 + x + \sqrt{(1-x)^2 + 4cx}\} \tag{9.8}$$

(see also [8]). Taylor expansion with respect to x gives then

$$\nu_l = -\sum_{k=1}^{l} (-1)^k \frac{(l+k-2)!\,c^k}{(k-1)!\,k!\,(l-k)!}. \tag{9.9}$$

As already mentioned before, these coefficients replace the coefficients given in (B7) that correspond to the exact expansion (4.5). The ν_l can be expressed in moments, i.e. they originate from elimination of summation constraints, just like in the exact case, where counting of diagrams yields the cumulants κ_l (see appendix A). The details of the procedure, as applied to the present case, are worked out in appendix C, where it is shown that the EMA propagator takes *all* (no less, no more) *self-consistent repeated ring diagrams* into account. It is different from the self-consistent repeated-ring approximation, which simply has a weight factor c for every (not nested) repeated-ring term. The proof proceeds as in appendix A, but starts from an expansion of the propagator from which *all* diagrams are excluded that are *not* of the nested ring type.

For a comparison between the exact case and the EMA, we have to consider equations (B4) and (B7) for the exact theory, and equations (C1) and (9.9), respectively, for the EMA. An analysis of these expressions as a function of c shows that the exact weights take on wildly varying values as c changes from 0 to 1 (symmetric around $c = \frac{1}{2}$, however), while the EMA weights do not exhibit this behaviour. This difference reflects the contributions of *non-ring* diagrams. The success of EMA in explaining the simulation data (see next section and [6] and [8]) could indicate that these non-ring contributions

cancel to a large degree. A comparison with recent exact results [21] shows that this is the case for the limit as $c \to 0$.

10. Results and discussion

We have tested the standard methods of kinetic theory, such as Boltzmann and ring equations, for calculating the diffusion coefficient $D(c)$ as a function of the density c of scatterers. A formal treatment of some approximation methods is given in the preceding sections. The general guiding principle for obtaining systematic approximations in orders of the density is to resum systematically (to a given order in the density) all diagrams with the most divergent time dependence, obtained from phase space estimates. Agreement and breakdown of these approximations in comparison with computer simulations have been fully explained on the basis of these methods. However, the present effective medium theory gives more. It provides, in a rather unexpected manner, a quantitatively correct theory for the density dependence of the diffusion coefficient over the entire density interval, also in cases where the other approximations break down. For this comparison of theory and computer simulations we refer to previous papers [6, 7, 8].

Let us first summarize how the diffusion coefficient is obtained for the different approximations. The EMA result in two dimensions is given by [6, 7, 8]

$$D = -\frac{1}{2ct_v^e} - \frac{1}{4} \tag{10.1}$$

where $t_v^e = t_1^e = t_2^e$ is the eigenvalue of the effective collision operator T^e for the eigenvectors $|V_\alpha\rangle$, i.e. the eigenvalue relevant for the velocity autocorrelation function [8] ($l = 3$ refers to the tensor eigenvalues, e.g. $t_3^e = t_t^e$). In the Boltzmann approximation t_v^e in (10.1) should be replaced by $t_v = -1 + \alpha - \beta$, as given below (2.10). The ring approximation is obtained by setting $t_l^e = t_l + t_l r_l t_l$ and the repeated-ring approximation by $t_l^e = t_l(1 - r_l t_l)^{-1}$, where r_l is the eigenvalue of the ring matrix (8.2). The self-consistent ring and repeated-ring approximations are similar, but with r_l and t_l^e determined self-consistently through iteration of the ring integral (8.2) with the propagator expressions (8.3) or (8.5), respectively. The EMA result is obtained by iteration of (8.2) and the EMA propagator (9.1), using (9.8). For the self-consistent approximations it is essential to realize that they involve both the vector eigenvalues and the tensor eigenvalues (i.e. $l = t$), as they are coupled through the ring eigenvalues.

For a more detailed discussion it is necessary to distinguish the cases with ($\beta \neq 0$) and without ($\beta = 0$) backscattering, respectively. We first consider models with $\beta = 0$, where computer simulations [8] show excellent agreement with the Boltzmann equation results for all densities. Here, the uncorrelated collisions yield the most divergent contributions and the Boltzmann equation results should therefore be correct as $c \to 0$. And so they do, as is seen in figure 6, where we plotted the results for the Boltzmann equation, the EMA (deviating less than 1% from the Boltzmann results [8]), and the ring approximations. Apparently, the RA, RRA, SRA, SRRA and EMA also provide *quantitatively correct* estimates for the slope of $cD(c)$ at low and high densities. This is somewhat surprising since none of these approximations accounts in a systematic manner for all most divergent diagrams to $\mathcal{O}(c)$. For instance, the orbiting collisions, illustrated in figure 2(c), have been neglected altogether. We have no explanation why

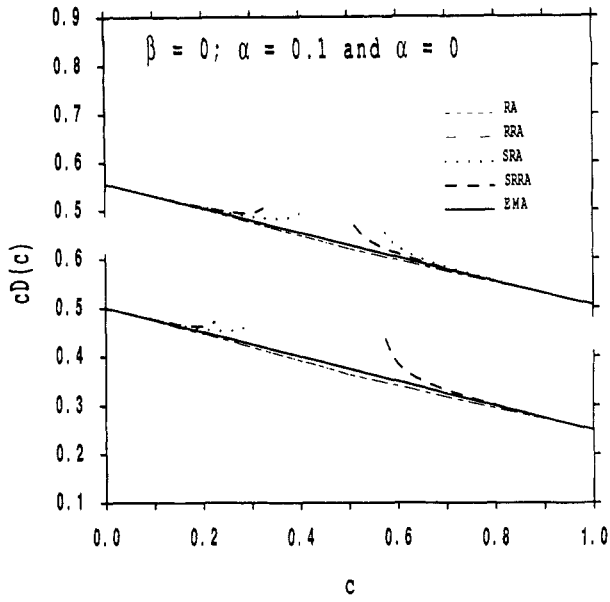

Figure 6. Comparison of several approximation schemes for some cases with zero reflection probability β. The upper set of curves is for $\alpha = \frac{1}{10}$, the lower for $\alpha = 0$. The EMA is practically identical to the Boltzmann appproximation. The RA and RRA practically coincide; the high-density SRA for $\alpha = 0$ is hidden in the other curves.

the results from the Boltzmann equation and the EMA agree so well over the entire density range. We also note that imposing self-consistency for the ring approximations unexpectedly induces stronger deviations from the Boltzmann and EMA results (see figure 6). One of the major results of the present work, however, is the identification of the events that are accounted for in EMA, where we stress that these results apply directly to the EMA that was initially developed for the bond percolation problem [3, 13, 14]. The (technical) proof of this is given in appendix C.

Next we consider the simulations and their predictions for the diffusion coefficient for Lorentz models *with backscattering*, i.e. $\beta \neq 0$, where EMA predictions agree very well with the simulations over the *entire* density range. At low densities the Boltzmann, R, RR and SR approximations yield totally incorrect results, whereas the low-density prediction of the SRRA and EMA are (to dominant order) in agreement with the simulations. The reason for agreement and deviations has been explained at the end of section 3 on the basis of phase space estimates. In figure 7 we plotted the results for the model with transition rates $\alpha = 0$, $\beta = \gamma = \frac{1}{3}$. As we showed previously [6, 8], the intercept of the EMA and SRRA with the $c = 0$-axis can be calculated analytically. We can show that the analogue for the SR approximation does not yield relevant results.

Also for models with reflections ($\beta \neq 0$), where the Boltzmann equation gives an entirely incorrect diffusion coefficient, it is not very clear why the EMA gives such accurate predictions of the diffusion coefficient for all densities. In order to investigate this, we performed some additional computer simulations at rather high values of the reflection probability β, up to $\beta = 0.95$. The simulations agree within error bars with EMA, just as for the model with $\beta = \gamma = \frac{1}{3}$. Apparently the diagrams that EMA does not account for, e.g. those that refer to backward/forward motion between two scatterers, cancel to a large degree. This can be understood by noting that, due to the strong

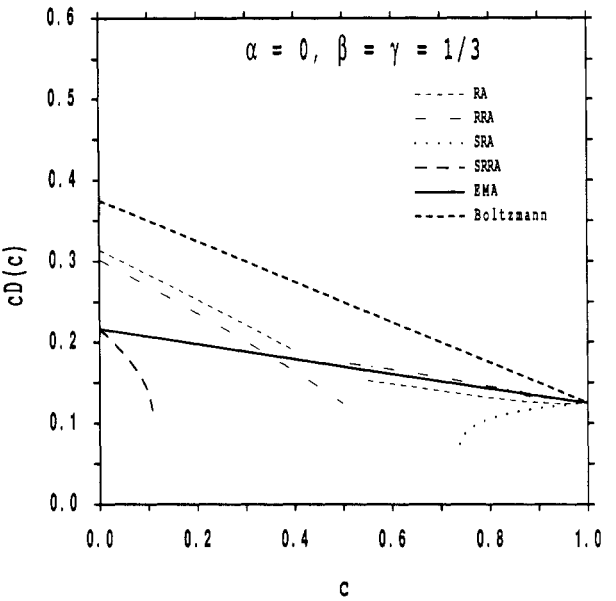

Figure 7. Comparison of approximations for a model with reflection.

reflections, the quasi one-dimensional features are enhanced. The cancellation of higher-order diagrams has been demonstrated before for a one-dimensional continuous Lorentz gas [33, 34]. Our comparison of simulation data with the EMA is in line with these results. Quite recently, the dominant low-density behaviour for the present model has been calculated exactly [21]; the results coincide with the low-density limit of the present EMA and the SRRA, and we conclude that for $c \to 0$ the non-(nested)-ring diagrams cancel.

It would be interesting to extend the present effective medium theory to different Lorentz lattice gases, such as the mirror model by Ruijgrok and Cohen [11, 32] and to the models with chiral scatterers of Gunn and Ortuño [9, 10]. Simulations of the mirror models with equal amounts of left and right oriented mirrors [32] show *positive* deviations from the Boltzmann results for the diffusion coefficient, whereas our stochastic Lorentz models show large *negative* deviations from Boltzmann. In extending the EMA to models with gyral scatterers it is also of interest to investigate whether EMA predicts (qualitatively) the existence of a percolation threshold, or at least a transition from extended orbits at small c to localized orbits at large c. Preliminary results obtained by the author indeed show a percolation threshold for the Gates model (only left-turning scatterers) at $c_p \sim 0.65$, which is to be compared with the, also preliminary, simulation result $c_p = 0.51$ [35].

The applications of the effective medium theory presented here and in [8] to these deterministic models are worked out in [36] and in a future paper.

Finally we note that the present stochastic Lorentz gas yields surprising results for the long-time tails in the velocity autocorrelation function (VACF). Even in models without backscattering, where D is correctly predicted by the Boltzmann and the ring and repeated-ring approximations, the long-time tail obtained from the R and RR approximation is incorrect, even to leading order in the density. The coefficient for the low-density tail, obtained from SRA, SRRA and EMA appears to be 50% to 100%

larger than that of the R and RR approximation, depending on the model parameters. We refer to [36] and [37] for an investigation of the long-time tails.

Appendix A. Exact weights

In this appendix we outline a constructive proof that the constraints on the summations in (3.3) and (4.3) are indeed eliminated if we replace the moments by the corresponding cumulants, defined in (3.4) and (4.4). The approach is an extension of the diagrammatic method for the one-dimensional disordered lattice [26], where the same weight factors occur as in the present expansion in Boltzmann propagators (4.3); the reason is that in both cases one has the bimodal distribution (2.1) for the c_n. We consider the expansion in terms of moments, of which the free propagator expansion is a special case ($\mu_l \to \mu_l^0 = c$ for all l). It is sufficient to show that a single weight μ_l is replaced by κ_l; it is then easily concluded that this implies that a product of moments μ is replaced by the product of the corresponding cumulants κ.

A term in the expansion (4.3) having only one factor, say, μ_l corresponds to l repeated returns to the same scatterer. Constraint summations that reduce to this diagram by dropping the constraints are those diagrams that correspond to partitions of l over different scatterers.

The objective here is to determine for every partition $(l_1, l_2, \ldots, l_m)$ of l, corresponding to diagrams with weight $\mu_{l_1}\mu_{l_2}\ldots\mu_{l_m}$, the factor $M_{l_1 l_2 \ldots l_m}$ in the replacement $\mu_l \to \mu_l + \ldots + M_{l_1 l_2 \ldots l_m}\mu_{l_1}\mu_{l_2}\ldots\mu_{l_m} + \ldots$. It will turn out that this modification is exactly the same as $\mu_l \to \kappa_l$.

First we write $\mu_{l_1}\mu_{l_2}\ldots\mu_{l_m}$ as $\mu_1^{n_1}\mu_2^{n_2}\ldots\mu_l^{n_l}$, where $\Sigma_i n_i = m$ and $\Sigma_i i n_i = l$ (obviously, $n_i = 0$ for $i > l$). Note that a term with this weight corresponds to *m different scatterers*. It is easily seen that for every set $\{n_i\}$ there are $l!/\Pi_i (i!)^{n_i} n_i!$ of these diagrams. (See also [39] 24.1.2). The replacement can now be written as $\mu_l \to X_l$ with

$$X_l = \sum_{m=1}^{\infty} \sum_{\{n_i\}}^{**} Y_m l! \prod_{i=1}^{\infty} \frac{1}{n_i!}\left(\frac{\mu_i}{i!}\right)^{n_i} \tag{A1}$$

with ** indicating the restrictions on the set $\{n_i\}$, given above. We will show that the Y_m are such that $X_l = \kappa_l$. So the remaining problem is to determine the Y_m. Clearly, $Y_1 = 1$ ($n_l = 1$, all other $n_i = 0$).

For illustration purposes we first consider the simple cases of two or three different scatterers. In the case of central moments (i.e. $\mu_1 = 0$) the quantity X_4 contains a term μ_4 and a term proportional to μ_2^2, referring to two different scatterers. There is one coincidence of site labels possible, resulting in $X_l = \mu_4 - 3\mu_2^2 (= \kappa_4)$, because there are three different diagrams with weight μ_2^2 (see the lower three lines of (4.3)). Similarly, $X_5 = \mu_5 - 10\mu_2\mu_3 (= \kappa_5)$, as there are 10 different diagrams with weight $\mu_2\mu_3$. The term proportional to say $\mu_2\mu_3\mu_4$ in X_9 ($m = 3$) is subtracted once from the first summation for the coincidence of all site labels, and 3 times from the summation over two distinct site labels. The latter, in turn, is subtracted once from the first summation (running over only one site label). The result is $-1-(-3) = +2$ and thus $X_9 = \ldots + 2 \times (9!)/(2!3!4!)\mu_2\mu_3\mu_4 + \ldots = \ldots + 2520\mu_2\mu_3\mu_4 + \ldots$.

Generally, the number of coincidences of initially m different scatterers is seen to be equal to the number of partitions of m into m_j subsets containing j species ($m = \Sigma_j j m_j$): $m!/\Pi_j m_j!(j!)^{m_j}$. (Example: coincidence of two of the m scatterers, keeping all the others different, can be achieved in $m!/2!(1!)^{m-1} = \frac{1}{2}m(m-1)$ ways.) Let

$k = m_1 + m_2 + \ldots + m_m$, then the partition $\{m_j\}$ refers to k different scatterers, with $k \leq m-1$, so we have reduced the problem to a sum of the same problems with a smaller number of different scatterers. It is clear that we have to subtract the quantity $m!/\Pi_j m_j!(j!)^{m_j}$ from the weights for diagrams with fewer different scatterers:

$$Y_m = -\sum_{k=1}^{m-1} \sum_{\{m_j\}}^{**} Y_k m! \prod_j \frac{1}{m_j!(j!)^{m_j}} = -\sum_{k=1}^{m-1} Y_k \mathscr{S}_m^{(k)} \tag{A2}$$

where ** indicates the restrictions $\Sigma_j j m_j = m$ and $\Sigma_j m_j = k$, and $\mathscr{S}_m^{(k)}$ is the Stirling number of the second kind (see [38], 24.1.2). Equation (A2) expresses Y_m in terms of all Y_k with $k < m$. Starting from $Y_1 = 1$, this is solved recursively. Using the relation $\mathscr{S}_{m+1}^{(k)} = k\mathscr{S}_m^{(k)} + \mathscr{S}_m^{(k-1)}$ [38], together with $\mathscr{S}_m^{(m)} = 1$ and $\mathscr{S}_m^{(0)} = \delta_{0m}$ we can write (A2), after some rearrangements, as

$$\sum_{k=1}^{m} (kY_k + Y_{k+1}) \mathscr{S}_m^{(k)} = 0. \tag{A3}$$

The part inside brackets does not depend on m. Starting from $m = 1$ and using that $\mathscr{S}_m^{(k)} \neq 0$ for $k \neq 0$, this equation yields $Y_{k+1} = -kY_k$, and with $Y_1 = 1$ we finally have

$$Y_m = (-1)^{m-1}(m-1)!. \tag{A4}$$

Substitution in (A1) and comparison with (B4) shows that the X_l are indeed the cumulants κ_l defined in (4.4).

Appendix B. Cumulants

In this appendix we derive the general expressions for the cumulants κ^0 and κ in terms of their moments and in terms of the concentration c. As an illustration we give the first few cumulants explicitly:

$$\begin{aligned} &\kappa_1^0 = c, \qquad \kappa_1 = 0, \qquad \kappa_2^0 = \kappa_2 = \mu_2 = c(1-c) \\ &\kappa_3^0 = \kappa_3 = \mu_3 = c(1-c)(1-2c) \\ &\kappa_4^0 = \kappa_4 = \mu_4 - 3\mu_2^2 = c(1-c)(1-6c+6c^2). \end{aligned} \tag{B1}$$

The general expressions for κ_l and κ_l^0 can be derived from the Taylor expansion of the logarithm in (4.4) and (3.4), respectively. We first do this for the general case, and then specialize to the κ_l^0. First we write

$$C(x) = \log F(x) = \sum_{k=1}^{\infty} \frac{(-1)^{k-1}}{k} \left(\sum_{l=1} \mu_l \frac{x^l}{l!} \right)^k. \tag{B2}$$

Using the multinomial expansion ([38], 24.1.2), this yields

$$C(x) = -\sum_{l=1}^{\infty} \frac{1}{l!} \sum_{k=1}^{l} \frac{k!l!x^l}{k} \sum_{\{n_i\}}^{**} \prod_i \frac{1}{n_i!} \left(\frac{-\mu_i}{i!} \right)^{n_i} \tag{B3}$$

and thus:

$$\kappa_l = -\sum_{k=1}^{l} (k-1)!l! \sum_{\{n_i\}}^{**} \prod_i \frac{1}{n_i!} \left(\frac{-\mu_i}{i!} \right)^{n_i} \tag{B4}$$

with the restrictions $\Sigma_i n_i = k$ and $\Sigma_i i n_i = l$ on the summations, and similar with κ_j and μ_j replaced by κ_j^0 and $\mu_j^0 = c$. This result can be used to evaluate the cumulants. In the case of κ_l^0 and μ_l^0, where $\mu_l^0 = \langle c_n^l \rangle = c$, we can take out the μ^0 from the last factor, yielding

$$\kappa_l^0 = -\sum_{k=1}^{l} (-c)^k (k-1)! \mathscr{S}_l^{(k)} \tag{B5}$$

where $\mathscr{S}_l^{(k)}$ is a Stirling number of the second kind (see [38], 24.1.2 and 24.1.4); it equals the number of ways of partitioning a set of l elements in k non-empty subsets:

$$\mathscr{S}_l^{(k)} = \sum_{m=0}^{k} (-1)^{k-m} \frac{m^l}{m!(k-m)!}. \tag{B6}$$

As $\kappa_l^0 = \kappa_l$ for $l \geq 2$, we can express the κ_l in terms of the concentration c:

$$\kappa_l = \kappa_l^0 = -\sum_{k=1}^{l} \sum_{m=1}^{k} (-1)^m \frac{(k-1)! m^l}{m!(k-m)!} c^k \tag{B7}$$

where the first equality is valid from $l = 2$ on.

Finally, we note that (3.4) and (4.4) yield for general $l \geq 2$ the low- and high-density limits of the cumulants:

$$\kappa_l = \kappa_l^0 = \begin{cases} c + c^2(1-2^{l-1}) + \ldots & c \to 0 \\ (-1)^l [p + p^2(1-2^{l-1}) + \ldots] & p = 1 - c \to 0. \end{cases} \tag{B8}$$

Appendix C. Nested-ring weights

We discuss the method that leads to an expression for the coefficients ν_l (equations (9.5), (9.7) and (9.9)), but now in terms of the moments μ_l. The reason for doing this is to make an identification of the diagrams that are accounted for by the effective medium approximation. The expression we derive yields (9.9) upon substitution of $\mu_l = \langle (\delta c_n)^l \rangle = c(1-c)^l + (1-c)(-c)^l$ or $\mu_l = \mu_l^0 = c^l$. The general idea is similar to the one used in appendix A; however, diagrams that are not of the (nested) ring type are systematically not accounted for. So we start from an expansion in Boltzmann propagators (cf. (4.3)) that only contains ring, repeated-ring and nested ring diagrams. For instance, the last term given explicitly in (4.3) is not of the nested (repeated) ring type, and therefore is absent in the present discussion. Consequently, as the other two terms collapse each in one way to a four-scatterer repeated-ring diagram, μ_4 is to be replaced by $\nu_4 = \mu_4 - 2\mu_2^2$, if we drop the summation constraints. Recall that the exact case gave $\kappa_4 = \mu_4 - 3\mu_2^2$. It is easily seen that in general a $\mu_i \mu_j$ term (requiring them to be of the nested-ring type, one sees that there are $l = i + j$ of them if $i \neq j$, or $\frac{1}{2}l$ if $i = j$) reduces in one way to an l-scatterer repeated-ring diagram, so the correction factor is $-l$.

For higher order diagrams we have to be more careful. We cannot simply consider (as in appendix A) the coincidences of a set of m scatterers, because some of them will not lead to nested ring type diagrams, even if we would start from one. See for example figure 8, where all three outcomes are to be considered in an *exact* formulation, but the lower one is not admitted here.

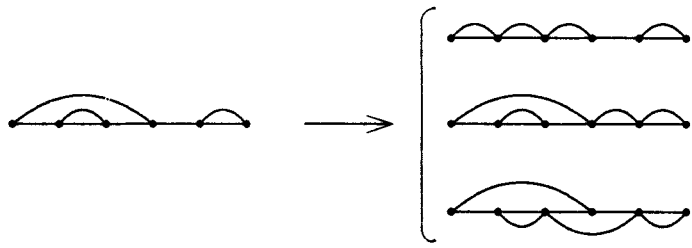

Figure 8. Diagrammatic representation of removing summation constraints. The last diagram is not of the nested-ring type.

Consider terms with weight $\mu_i\mu_j\mu_k$; if $i \neq j \neq k \neq i$, there are $l(l-1)$ ring diagrams with this weight (it is equivalent to indicating the separation points between the first and second, and between the second and third scatterer on an l element chain. Subsequently filling up the whole chain yields a nested ring diagram.) For each of these $l(l-1)$ diagrams we determine by counting in how many ways one can make a nested ring diagram of two different scatterers. The latter, in turn, reduce to one-scatterer diagrams in one way each. The total correction factor then appears to be $+l(l+1)$, apart from a factor $1/(2!)$ or $1/(3!)$ if i, j and/or k happen to be the same.

In the case of initially four different scatterers, we determined the correction factor to be $-l(l+1)(l+2)$. We note that for higher order cases the number of possibilities rapidly increases, and the enumeration becomes more and more elaborate.

From these low-order examples we predict that in general for k different scatterers out of l, the correction factor is $-(-1)^k(l+k-2)!/(l-1)!$, and the ν_l are expressed in moments by

$$\nu_l = -\sum_{k=1}^{\infty} \sum_{\{n_i\}}^{**} \frac{(l+k-2)!}{(l-1)!} \prod_{i=1}^{\infty} \frac{(-\mu_i)^{n_i}}{n_i!} \tag{C1}$$

with constraints $\Sigma_i\, in_i = l$ and $\Sigma_i\, n_i = k$.

The above analysis was carried out for the case of central moments $\mu_l = \langle(\delta c_n)^l\rangle$, i.e. no diagram contains isolated T-vertices. However, it also holds for the moments $\mu_l^0 = \langle c_n^l\rangle = c$ (compare appendices A and B), in which case we recover (9.9). To prove the validity of (C1) we insert $\mu_l^0 = c$ and compare the coefficient of c^k with that in (9.9). This requires the equality

$$a_{lk} \equiv \sum_{\{n_i\}}^{**} \prod_{i=1}^{\infty} \frac{1}{n_i!} = \frac{(l-1)!}{(k-1)!\,k!\,(l-k)!} \tag{C2}$$

The equality is proved by means of generating functions

$$F(x,y) = \sum_{l,k=0} a_{lk} x^l y^k = \exp\left(\frac{xy}{1-x}\right) \tag{C3}$$

where the RHS is obtained from the first equality in (C2). Expanding this again, using the multinomial formula for $(1-x)^{-m}$ with $\binom{-m}{n} = (-1)^n(m+n-1)!/(n!(m-1)!)$, the RHS of (C2) follows. This shows that (C1) is valid both for the moments μ_l^0 and for the central moments μ_l.

Summarizing, we have indicated a procedure that explains the weight factors occurring in the effective medium approximation (EMA), based on a propagator expansion in which all *non-nested ring diagrams* are systematically *neglected.*

Acknowledgements

The author wants to thank M H Ernst for the fruitful collaboration during the preparation of this paper. He also wishes to thank E G D Cohen for some interesting discussions, and is further indebted to H van Beijeren for some critical remarks on the manuscript. The work of the author is financially supported by the Stichting voor Fundamenteel Onderzoek der Materie (FOM), which is sponsored by NWO.

References

[1] Wolfram S 1984 *Rev. Mod. Phys.* **55** 601
Wolfram S (ed) 1986 *Theory and Applications of Cellular Automata* (Singapore: World Scientific)
[2] Frisch U, d'Humières D, Hasslacher B, Lallemand P, Pomeau Y and Rivet J P 1987 *Complex Systems* **1** 649
Henon M 1987 *Complex Systems* **1** 763
Rivet J P 1987 *Complex Systems* **1** 839
[3] Kirkpatrick S 1973 *Rev. Mod. Phys.* **45** 574
[4] Haus J W and Kehr K W 1987 *Phys. Rep.* **150** 263
[5] Hauge E H 1974 *Transport Phenomena* (*Lecture Notes in Physics* **31**) ed G Kirczenow and J Marro (Berlin: Springer) p 338
[6] Ernst M H, van Velzen G A and Binder P M 1989 *Phys. Rev.* A **39** 4327
[7] van Velzen G A and Ernst M H 1988 *Workshop on Discrete Kinetic Theory, Lattice Gas Dynamics and Foundations of Hydrodynamics (Turin, 1988)* ed R. Monaco (Singapore: World Scientific)
[8] Ernst M H and van Velzen G A 1989 *J. Phys. A: Math. Gen.* **22** 4611-32.
[9] Gunn J M F and Ortuño M 1985 *J. Phys. A: Math. Gen.* **18** L1095
[10] Gates D J 1972 *J. Math. Phys.* **13** 1005; 1972 *J. Math. Phys.* **13** 1315
[11] Ruijgrok Th W and Cohen E G D 1988 *Phys. Lett.* A **133** 415
[12] Binder P M 1987 *Complex Systems* **1** 559
[13] Webman I 1981 *Phys. Rev. Lett.* **47** 1496
[14] van Velzen G A, Ernst M H and Dufty J W 1988 *Physica* **154A** 34
[15] McLennan J A 1989 *Introduction to Non-equilibrium Statistical Mechanics* (Englewood Cliffs, NJ: Prentice Hall)
[16] Dorfman J R and van Beijeren H 1977 ed B J Berne *Statistical Mechanics, Part B: Time dependent processes* (New York: Plenum) p 65
[17] Senger J V and Gillespie D T 1977 ed B J Berne *Statistical Mechanics, Part B: Time dependent processes* (New York: Plenum) p 65
[18] Bruin C 1972 *Phys. Rev. Lett.* **29** 1670; 1974 *Physica* **72** 261
[19] van Leeuwen J M J and Weyland A 1967 *Physica* **36A** 457
Weyland A and van Leeuwen J M J 1968 *Physica* **38A** 35
[20] Hauge E H and Cohen E G D 1969 *J. Math. Phys.* **10** 397
[21] van Beijeren H private communication
[22] Ernst M H and Binder P M 1988 *J. Stat. Phys.* **51** 981
[23] van Kampen N G 1981 *Stochastic Processes in Physics and Chemistry* (Amsterdam: North Holland)
[24] Okamura Y, Blaisten-Barojas E and Fujita S 1980 *Phys. Rev.* B **22** 1638
[25] Fujita S, Okamura Y, Blaisten E and Godoy S V 1980 *J. Chem. Phys.* **73** 4569
[26] Denteneer P and Ernst M H 1983 *J. Phys. C: Solid State Phys.* **16** L961; 1984 *Phys. Rev.* B **29** 1755
[27] Ernst M H, van Velthoven P F J and Nieuwenhuizen Th M 1987 *J. Phys. A: Math. Gen.* **20** 949
[28] Ernst M H 1987 *J. Stat. Phys.* **48** 645
[29] van Velzen G A and Ernst M H 1987 *J. Stat. Phys.* **48** 677

[30] Domb C and Fisher M E 1958 *Proc. Camb. Phil. Soc.* **54** 48
[31] Odagaki T, Lax M and Puri A 1983 *Phys. Rev.* B **28** 2755
[32] Kong X P and Cohen E G D 1989 *Phys. Rev.* B **40** 4838
[33] van Beijeren H 1982 *Rev. Mod. Phys.* **54** 195
van Beijeren H and Spohn H 1983 *J. Stat. Phys.* **31** 231
[34] Grassberger P 1980 *Physica* **103A** 558
[35] Bouwens B Th 1989 *Report*, University of Utrecht, unpublished
[36] van Velzen G A 1990 *PhD Thesis* University of Utrecht, February 1990
[37] Ernst M H and van Velzen G A 1989 *J. Stat. Phys.* **57** 455-72
[38] Abramowitz M and Stegun I A 1970 *Handbook of Mathematical Functions* (New York: Dover)